DOE/SERI-9234/1

PHOTOVOLTAIC MECHANISMS IN POLYCRYSTALLINE THIN FILM SILICON SOLAR CELLS

Quarterly Technical Progress Report No. 1, July 30—October 31, 1980

By
Bhushan Sopori

Work Performed Under Contract No. AC02-77CH00178

Motorola, Inc.
Solar Energy Department
Phoenix, Arizona

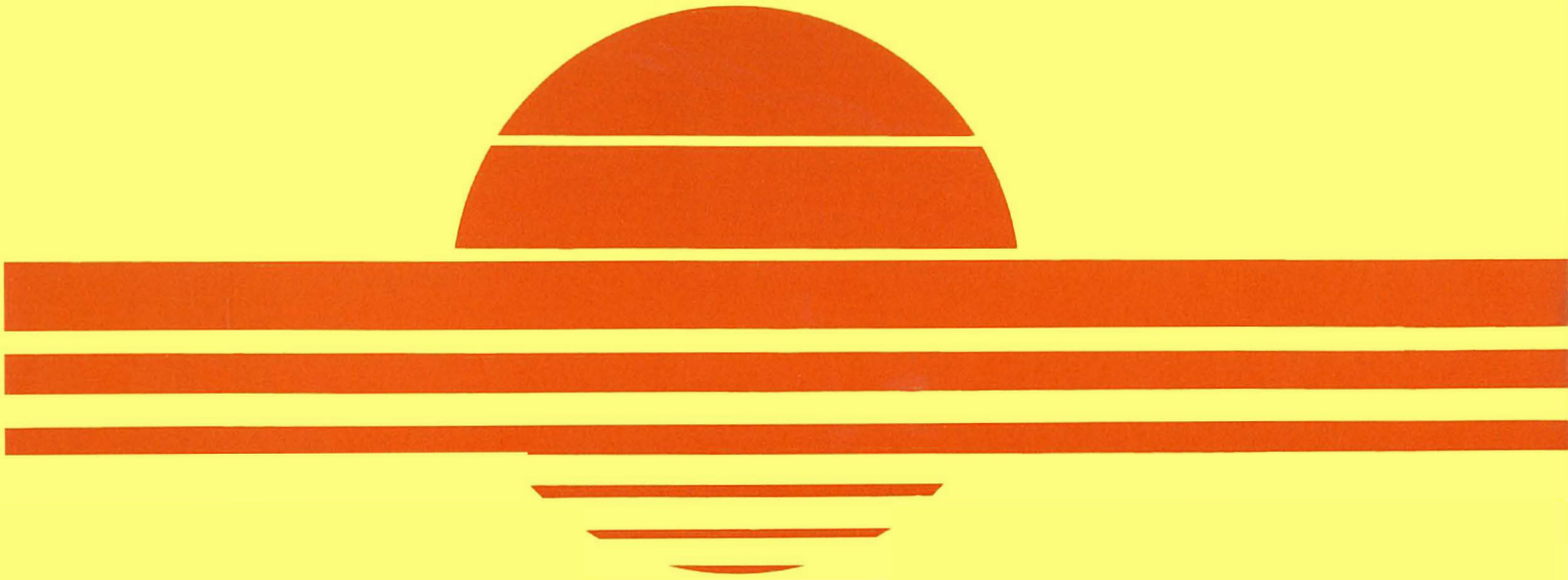

U.S. Department of Energy

Solar Energy

DISCLAIMER

Available from the National Technical Information Service, U. S. Department of Commerce, Springfield, Virginia 22161.

Price: Printed Copy A03
Microfiche A01

DOE/SERI-9234/1
Distribution Category UC-63

PHOTOVOLTAIC MECHANISMS IN POLYCRYSTALLINE THIN FILM SILICON SOLAR CELLS

QUARTERLY TECHNICAL PROGRESS REPORT NO. 1

FOR PERIOD

30 JULY 1980 - 31 OCTOBER 1980

BHUSHAN SOPORI

SUB-CONTRACT NO. XZ-0-9234

START DATE 7/30/80
COMPLETION DATE 8/29/81

PREPARED BY

MOTOROLA, INC.
SOLAR ENERGY DEPARTMENT
5005 EAST McDOWELL ROAD
PHOENIX, ARIZONA 85008

PREPARED FOR

UNITED STATES
DEPARTMENT OF ENERGY
DIVISION OF SOLAR TECHNOLOGY
AND
SOLAR ENERGY RESEARCH INSTITUTE

MOTOROLA PROJECT NO. 2386

TABLE OF CONTENTS

LIST OF FIGURES

LIST OF TABLES

1.0 OBJECTIVES OF THE PROGRAM

1. Development of the surface preparation techniques to aid in the unequivocal interpretation of grain boundary (G.B.) data.
2. Characterization of G.B.s in terms of chemical, physical, electrical and optical parameters, and correlation to solar cell performance.
3. Identification of the effects of intra grain crystal defects and
4. Determination of effects of solar cell processing on G.B. parameters and bulk defects.

2.0 ABSTRACT

Major accomplishments, during the first quarter of the contract period were in the following areas:

1. Small area diode fabrication and analysis has been continued. This technique has further been applied to many RTR ribbons.
2. An optical technique for determination of crystallite orientations has been placed in operation. This technique has many distinct advantages. These are: (i) rapid (ii) can be set-up very inexpensively, (iii) well suited for polycrystalline substrates of small grain size and (iv) can easily characterize twins. Accuracies obtained with this technique are about the same as that of the Laue technique.
3. A technique to qualitatively evaluate grain boundary activity in unprocessed substrates has been used and valuable results obtained. Further analysis is being done to use this technique for quantitative evaluation.
4. A major study of G.B. orientation effects is underway. Initial results on RTR ribbons have shown a good correlation of G.B. barrier height with misorientation (tilt boundaries).

3.0 INTRODUCTION

Several techniques are being studied to determine: (i) effects of grain orientations on photovoltaic properties and (ii) the dependence of photovoltaic losses on grain boundary (G.B.) misfit. These include (a) an optical technique for determination of crystal orientations and (b) an optical technique to determine G.B. "activity" in substrates having no P-N junctions. These techniques have been applied to investigate orientation and G.B. effects in RTR ribbons. Results obtained have shown a good correlation between misfit and "activity" at the G.B. Furthermore, recombination and barrier effects due to twin boundaries and G.B.s have been identified.

4.0 AN OPTICAL DIFFRACTION TECHNIQUE FOR DETERMINATION OF CRYSTAL ORIENTATIONS

Conventionally, crystal orientations are determined by x-ray techniques such as Laue patterns and diffractometry. We here investigate a new optical technique which appears to be a powerful, yet simple, method for determination of crystal orientations. This technique utilizes the fact that certain crystallographic etchants can generate pseudo-periodic structures on the surfaces of single or large grain polycrystalline samples. Such an etched surface then behaves much like a two-dimensional grating, with a groove shape which is characteristic of the crystal orientation. If the surface is illuminated with monochromatic light, such as a HeNe laser, a diffraction pattern characteristic of surface orientation can be observed.

Work that we have done on silicon indicates that such a technique is, indeed, very useful. Advantages of this technique, as compared to the Laue method are: (i) simplicity (ii) rapidity of measurement, and (iii) suitability for polycrystalline substrates. The accuracy of this technique is comparable to that of the Laue method. It should be emphasized that the present technique differs from some other optical techniques used previously for alignment of single crystal ingots that are based on incoherent reflections from etch pits (1,2). Since the present technique utilizes the periodic nature of the surface texture, it is possible to analyze theoretically the diffraction patterns to determine crystal orientations in terms of the parameters of the diffraction patterns. Furthermore, the observed patterns are of high quality, requiring only a low power source (e.g., a few mW output HeNe laser).

Determination of crystal orientation by this technique involves two steps:
(a) texture etching to generate a two-dimensional grating pattern, and
(b) evaluation of diffraction parameters such as the geometry of the far-field pattern and the angular deviation of the diffracted beams. These are described for single and polycrystalline silicon samples.

4.1 TEXTURE ETCHING

Texture etching is a technique recently developed for reducing surface reflections from (100) oriented silicon surfaces (3-5). A major application is in solar cell fabrication where texturing in conjunction with a single layer A.R. coating, offers a method for production of broad band antireflection. Several etchants are known to "texture" silicon surfaces. These include hydrazine (N_2H_4) and sodium or potassium based hydroxides.

Texturing forms surface structures whose shape depends on surface orientation. For a known orientation, the characteristic groove shape can be determined from a knowledge of etch rates for different directions. For example, for low index planes, the etch rate, R, varies as:

$$R_{<111>} < R_{<110>} < R_{<100>}$$

Shapes for three major orientations in silicon are shown in Fig. 1. Figure 2 shows photographs of the surface structures formed by texture etching <100>, <110> and <111> oriented silicon samples. The crystal symmetries of these orientations are reflected in the symmetries of the grating configurations. Other orientations will in general lead to asymmetric grating configurations. A simple way of determining groove shape for any given orientation is to determine the angular offset of this crystal plane from low index planes; from a knowledge of angular offsets and the grating shapes for low index orientations, one can determine the grating shape for the given orientation. This procedure is explained further by an example given later.

It should be pointed out that texturing can be controlled to generate a highly regular surface structure essential to high quality diffraction patterns. We have found that the regularity of the pattern is a function of the peak height of the surface structure. Most desirable structures are obtained when the texturing is adjusted to give (100) surfaces with a peak height of ~15μm.

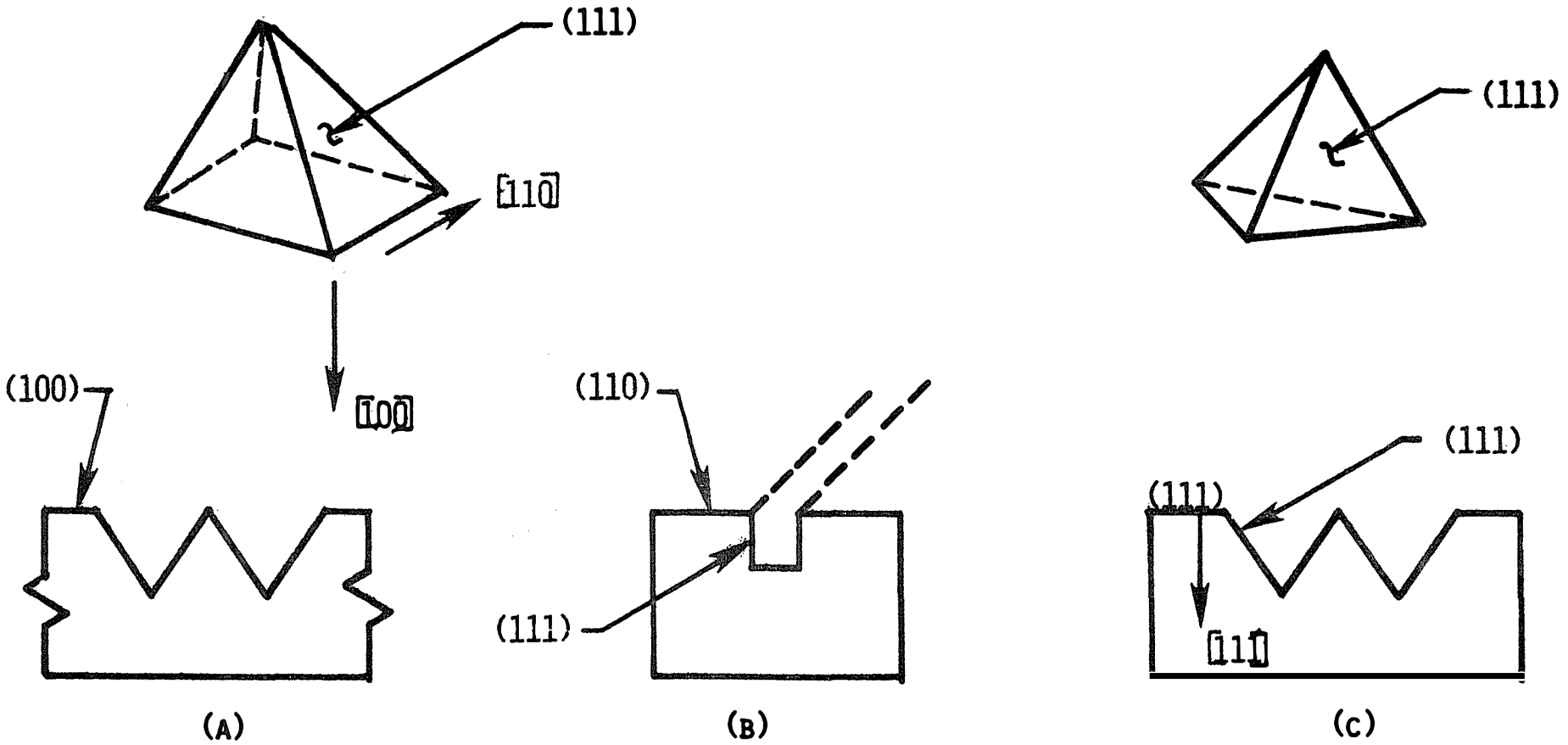

FIGURE 1: GRATING SHAPES FOR THREE LOW INDEX ORIENTATIONS (A) (100) (B) (110) AND (C) (111).

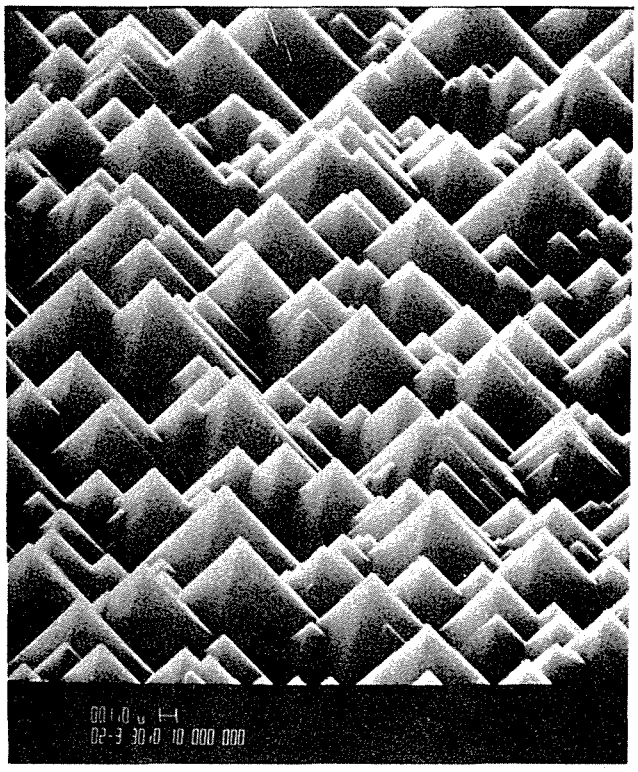

(a) SEM photograph

Figure 2: Photographs of surface structures on (a) (100) (b) (110) and (c) (111) orientation formed by texture etching.

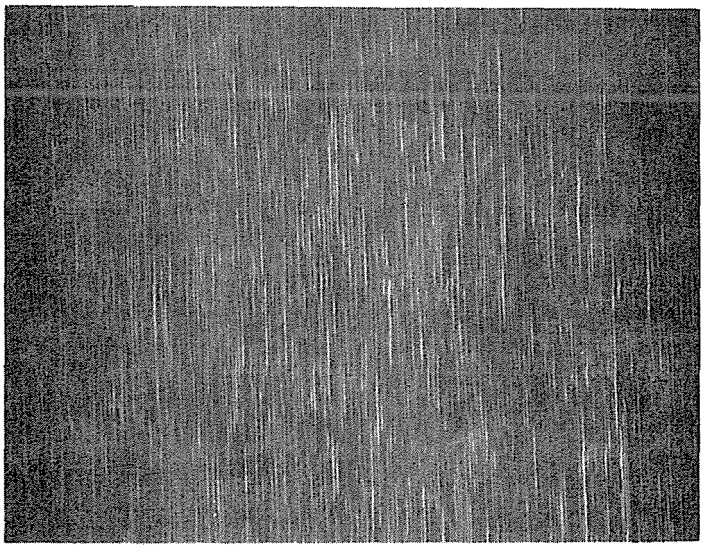

(b) Optical Micrograph, Magnification = 400X

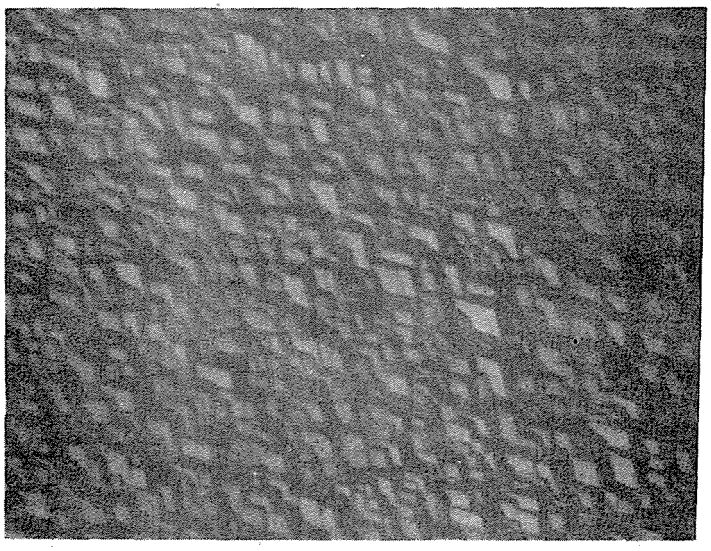

(c) Optical Micrograph, Magnification = 400X

Figure 2: (continued)

4.2 EVALUATION OF DIFFRACTION PATTERNS

Diffraction patterns are obtained by illuminating the textured sample with a HeNe laser beam (λ = 6328Å). Figure 3 shows a schematic of the equipment used for observing and analyzing the far-field diffraction patterns in reflection. The sample is vacuum mounted on a goniometric arrangement which allows the sample to be rotated in horizontal and vertical planes. A light beam, after passing through a hole in the screen, is incident on the sample so that it coincides with the intersection of the goniometer axes. This allows angular adjustments of the sample without changing either the position of the light beam on the sample or the distance between sample and screen. Diffraction patterns may be viewed directly on the screen or photographed using a translucent screen as shown in the figure. The screen itself may be marked with loci of constant angles subtended with the sample (for a constant sample-to-screen distance) to facilitate measurements which are described later.

Diffraction patterns due to <100>, <110> and <111> silicon surfaces, for near normal incidence of light, are shown in Fig. 4a, 4b, and 4c respectively. Diffraction patterns due to <110> and <111> are shown for slightly off normal incidence in order to avoid elimination of the central part of the pattern by the aperture in the screen. Crystal symmetries of these orientations are clearly seen from the diffraction patterns. For oblique incidence, diffraction patterns may differ significantly from those of normal incidence and, additionally, become asymmetric. Figures 5a and 5b show diffraction patterns of a (100) oriented surface illuminated at 25° and 65° respectively. Notice that in Fig. 5b most of the energy is contained in a single diffraction order. Patterns similar to those shown in Fig. 5 are obtained if the sample orientation is such that the surface is illuminated at normal incidence but is inclined with respect to a (100) plane.

Diffraction patterns (as seen in Fig. 4 and 5) are characterized by two parameters which are directly related to crystal orientation. These are:

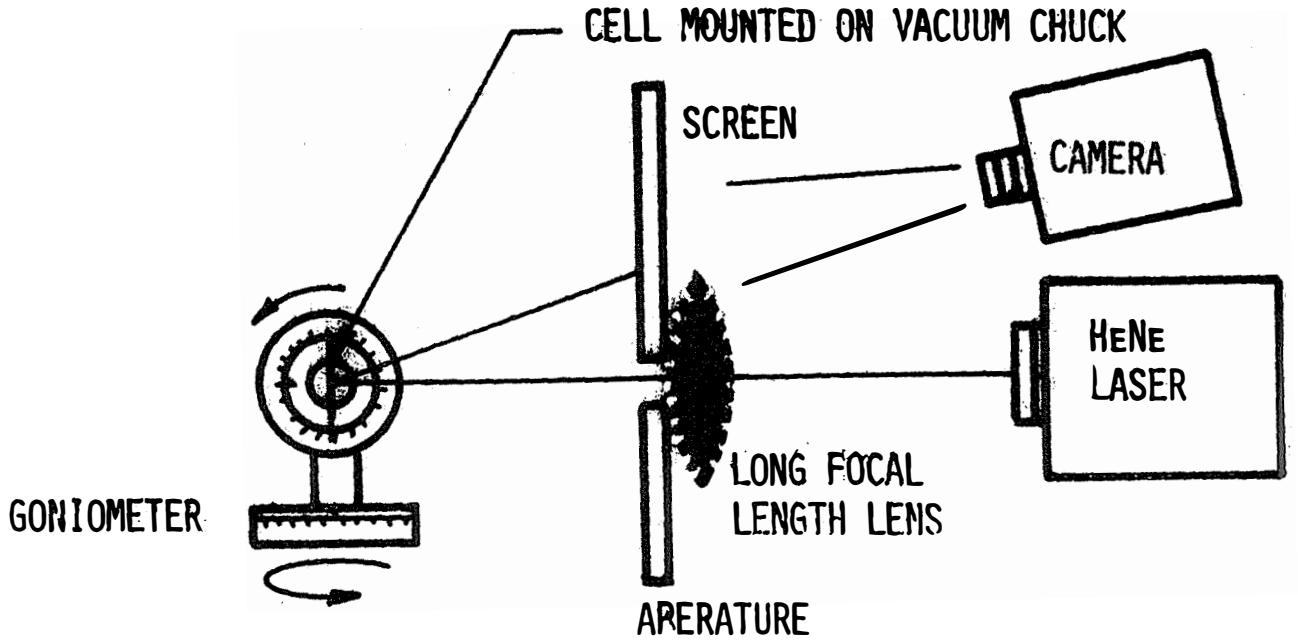

FIGURE 3: SCHEMATIC OF A SET-UP FOR OBSERVATION AND ANALYSIS OF DIFFRACTION PATTERNS.

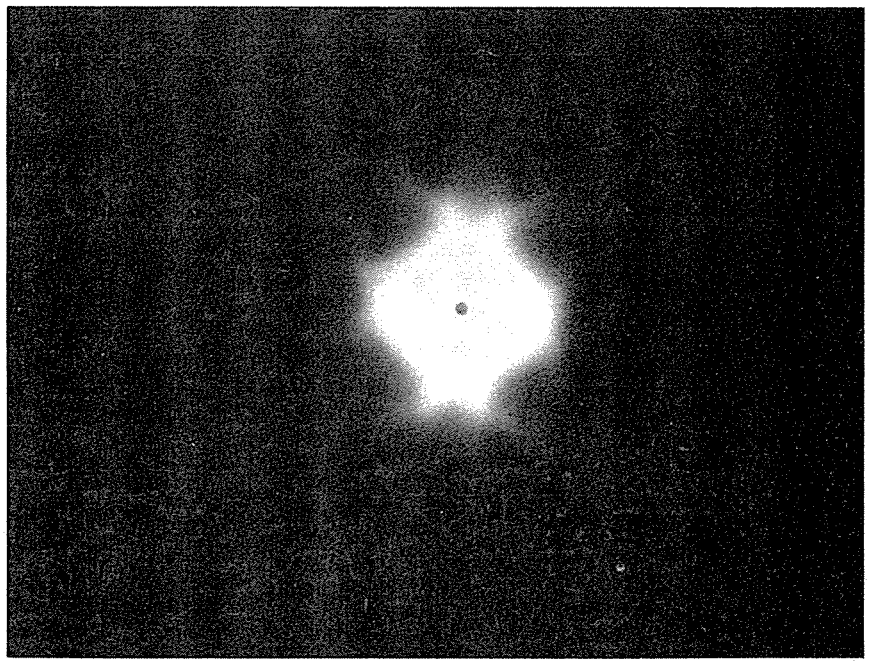

(a)

Figure 4: Diffraction patterns due to textured silicon wafers of the following orientations: (a) (100) (b) (110) and (c) (111).

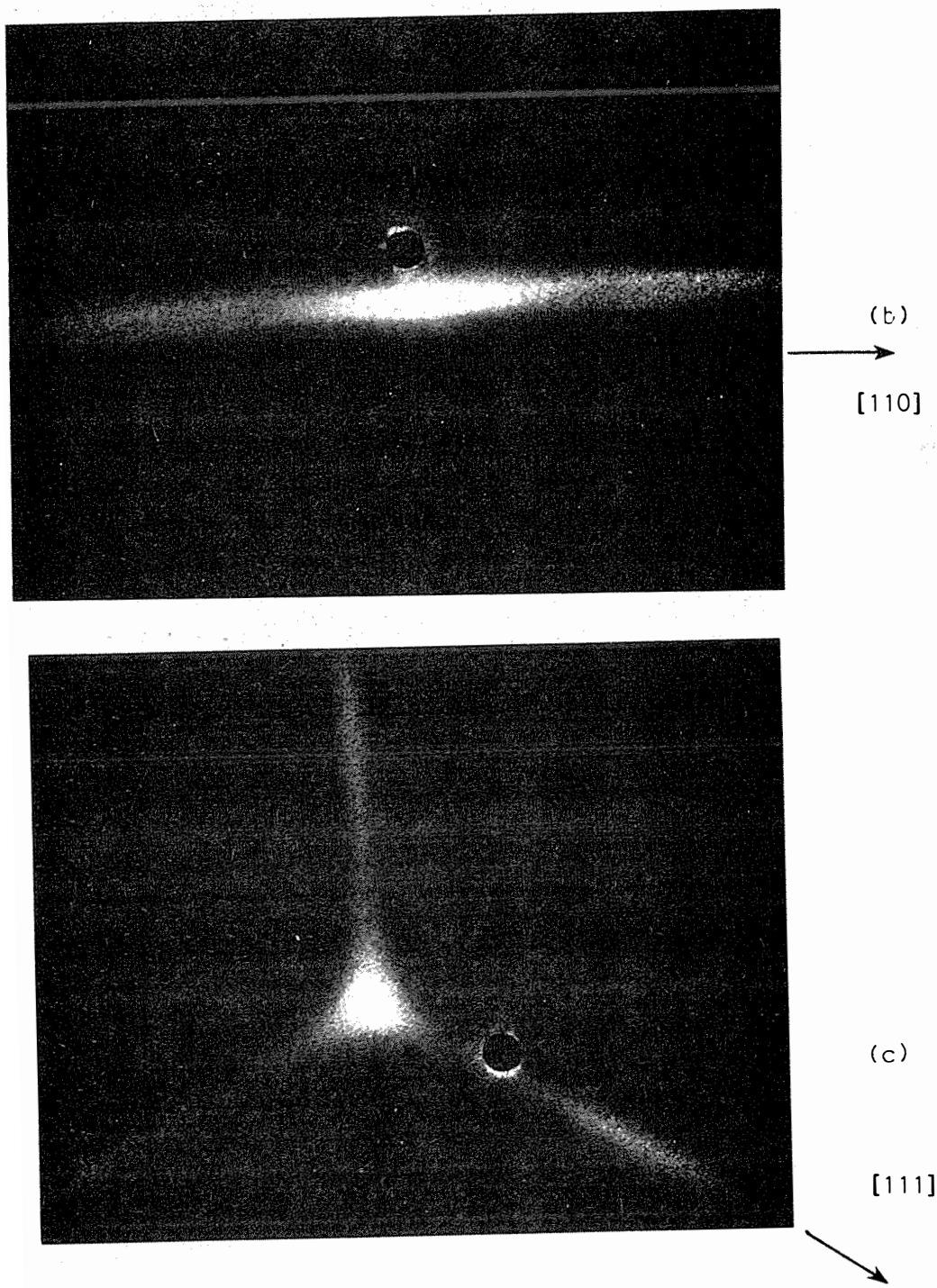

Figure 4: (continued)

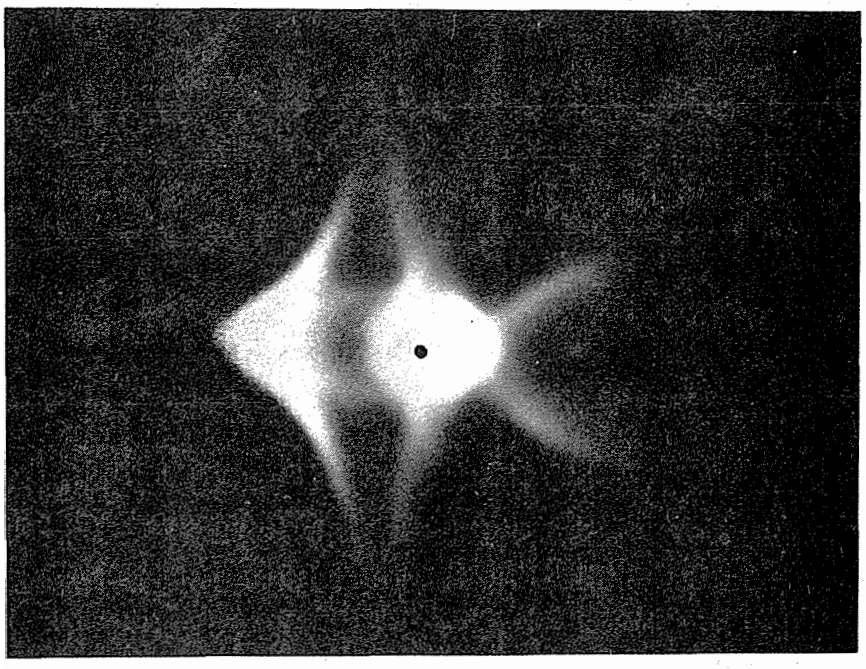

(a)

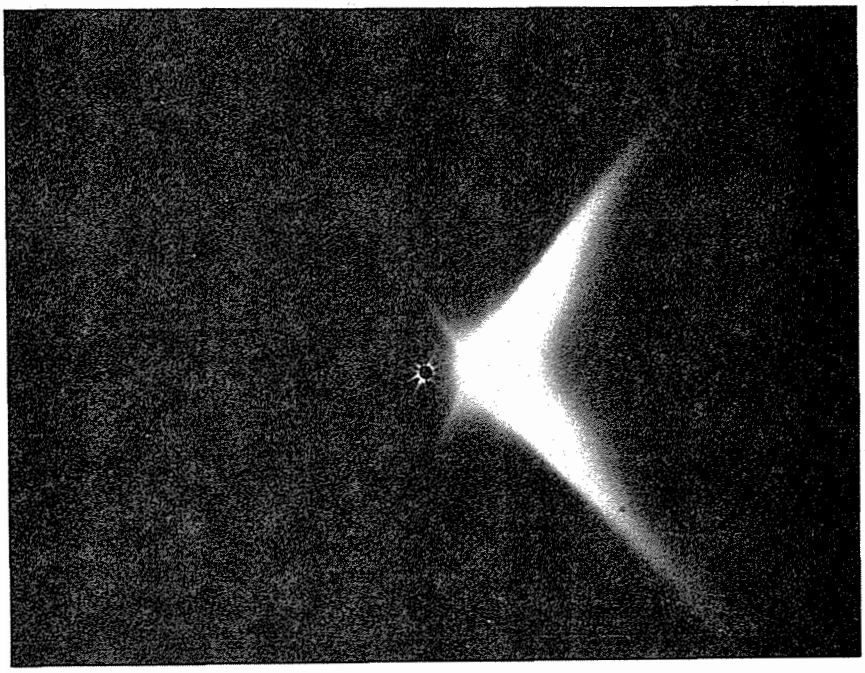

(b)

Figure 5: Diffraction patterns due to a (100) textured silicon wafer for oblique incidence. Incident angles are: (a) 25° (b) 65°.

(1) the shape of the various lobes of the pattern, and (2) the angular deviation of the lobes, particularly the dominant ones. We have developed a theoretical treatment to relate diffraction parameters to groove shape and hence to crystal orientation. This theory leads to a simple step-by-step procedure for determination of orientation (6).

The approach of this analysis, as noted earlier, is that the orientation of the surface may be described in terms of angular deviations, $\Delta\theta$ and $\Delta\phi$, of the surface plane with respect to one (or more) low index planes such as (100), (110), and (111), where $\Delta\theta$ and $\Delta\phi$ are measured in terms of rotations with respect to two orthogonal axes (7). This approach has practical significance in that when a sample of unknown orientation is illuminated at normal incidence, a diffraction pattern reminiscent of some low index plane can easily be recognized even for large $\Delta\theta$ and $\Delta\phi$. Once this low index pattern is recognized, $\Delta\theta$ and $\Delta\phi$ can be determined from angular readjustment of the sample orientation with respect to the incident beam. The angular readjustment is done such that one of the dominant lobes is reflected parallel to the incident beam. The following example will illustrate the principle involved in this procedure.

Let us consider a (100) oriented silicon wafer textured to give a grating shape shown in Fig. 1. This groove shape may be redrawn for convenience, as shown in Fig. 6, as a projection on a (100) plane, to indicate two orthogonal grating structures along the x and y directions. It can be shown that the total diffraction pattern can be regarded as a sum of diffraction patterns due to gratings along x and y directions (6). A one-dimensional grating model, Fig. 6b, can be used to determine the angular deviation of lobes due to each grating component based on a ray optics approach. This angle is found to be 39.2°, agreeing well with the measured value. Let us now consider a special case in which the sample is

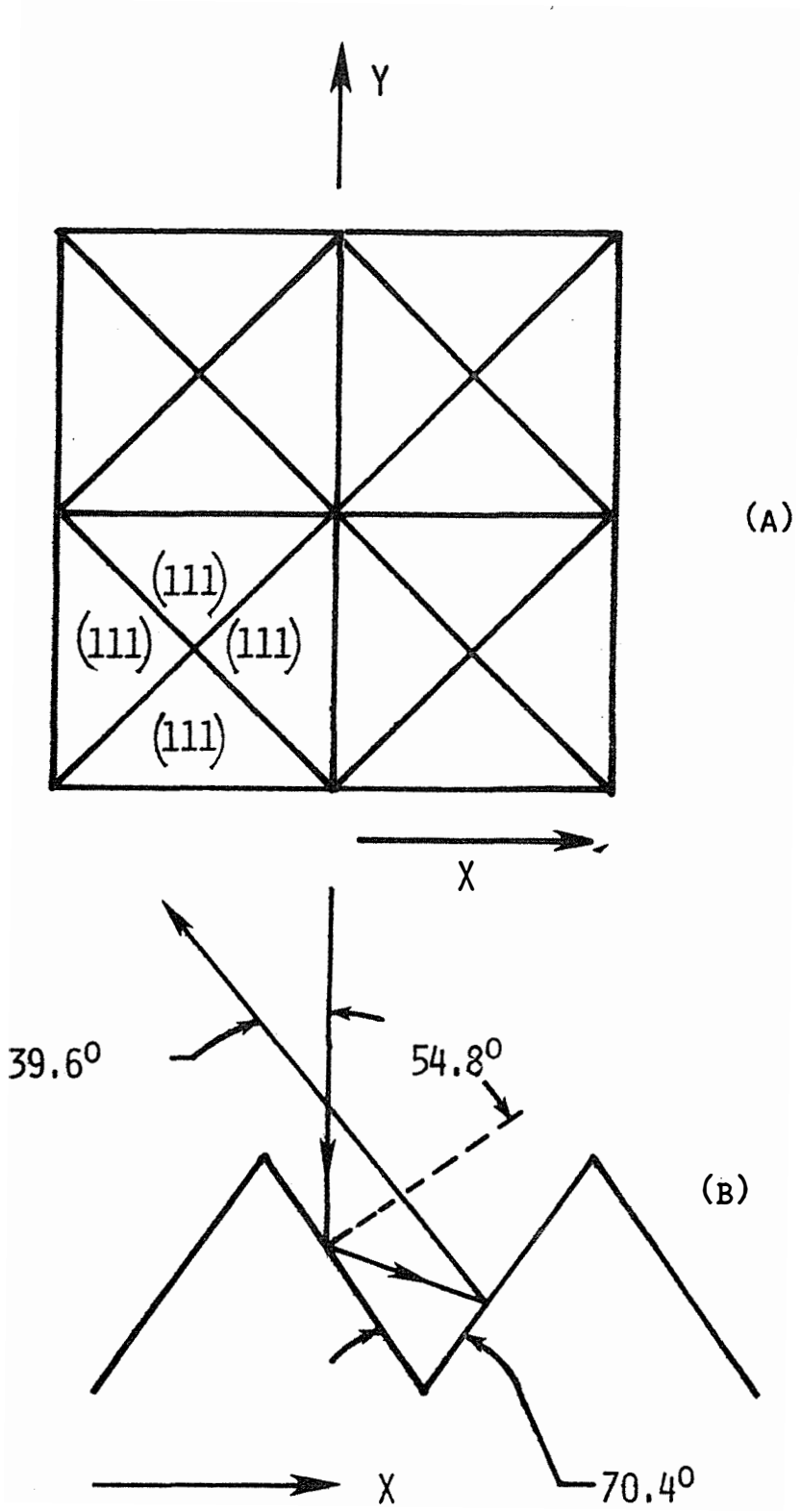

FIGURE 6: (A) PROJECTION OF THE GRATING STRUCTURE ON THE (100) PLANE SHOWING X AND Y COMPONENTS (B) ONE DIMENSIONAL GRATING COMPONENT OF (A).

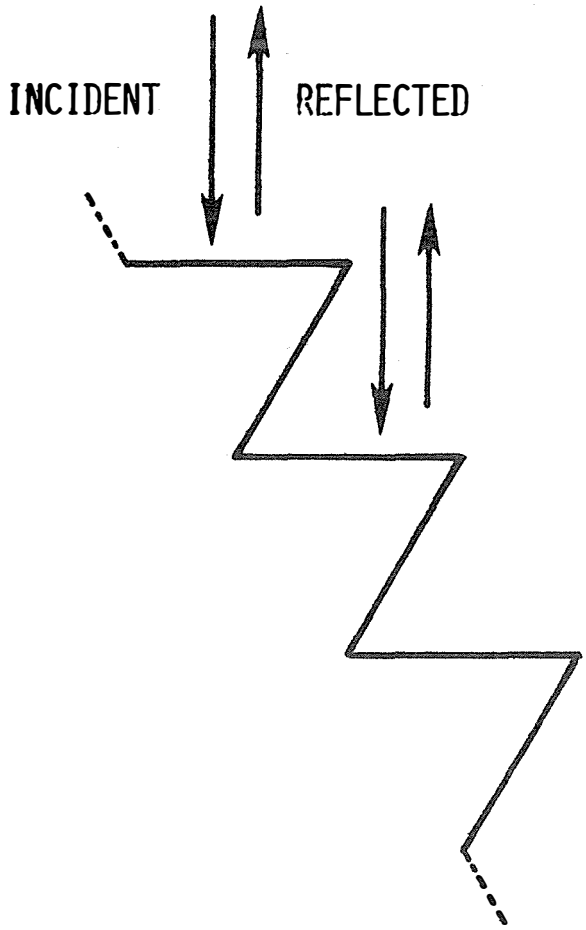

FIGURE 6c: SKETCH SHOWING X-COMPONENT OF GRATING IN ECHELETTE CONFIGURATION: LIGHT IS INCIDENT NORMALLY ON ONE FACE OF THE GRATING. RESULTANT DIFFRACTION PATTERN IS SIMILAR TO FIGURE 5B.

rotated through 54.8° about one of the (110) axis. Figure 6c shows this grating configuration. Notice that this is similar to an echelette grating and that the diffraction pattern due to the x-component of the grating will be a single lobe (8). Conversely, this condition can be used to determine the angle between the sample surface and (111) planes of the grating.

Now, consider a sample with a surface inclined with respect to (100) planes at angles $\Delta\theta$ and $\Delta\phi$, as shown in Fig. 7a. When this sample is texture etched, the grating shape will be asymmetric. The (111) planes along the x-direction will be inclined with respect to the surface at an angle of $54.8^{\circ} \pm \Delta\theta$, and along the y-direction at $54.8^{\circ} \pm \Delta\phi$. Figure 7b shows the resultant shape in the x-direction. Results of these changes in the groove shape will change both the intensity and angular distribution of the diffraction pattern. Note that $\Delta\phi$ will also cause each lobe due to the x-component of the grating to be asymmetric. Although these changes are related to $\Delta\theta$ and $\Delta\phi$, a more practical procedure to determine $\Delta\theta$ and $\Delta\phi$ directly is to rotate the sample on the goniometric stage such that a dominant lobe is in the direction of the incident beam as described in the previous paragraph. In this case the orientation of the surface is: $\Delta\theta \pm 54.8^{\circ}$ with respect to a (100) plane.

From the previous discussion we see that the determination of the crystal orientation from a diffraction pattern involves two steps: (1) recognition of the reminiscent pattern of a low index plane, and (2) determination of angles $\Delta\theta$ and $\Delta\phi$ required to cause the characteristic lobes of the pattern to be collinear with the incident beam.

This technique can also be used to determine grain orientations in polycrystalline samples. An additional advantage of this technique is an easy

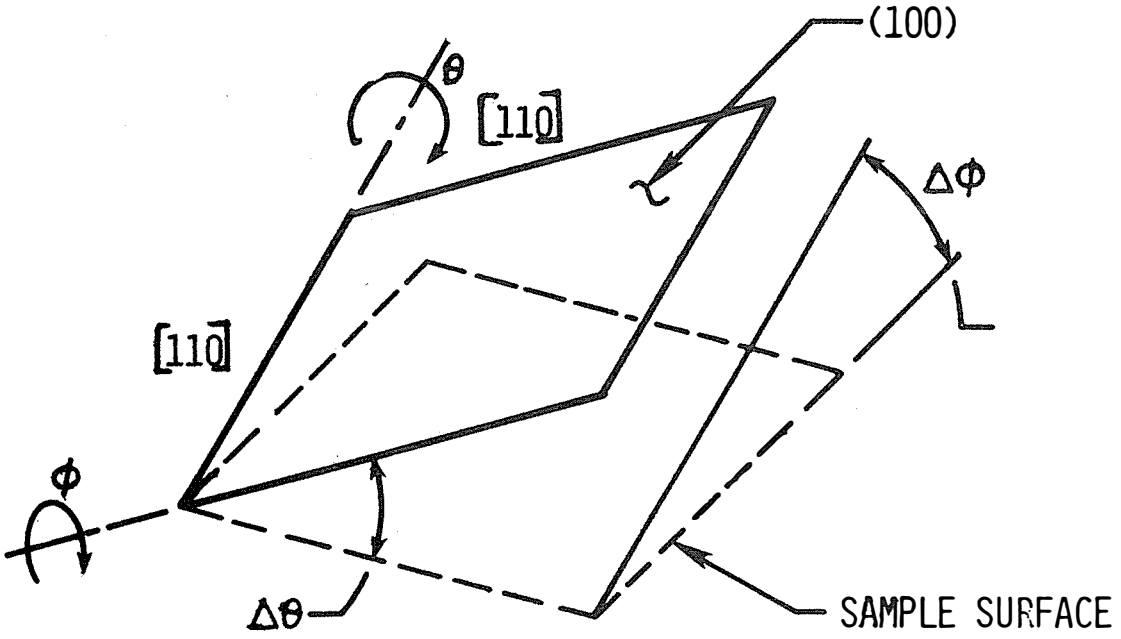

(A)

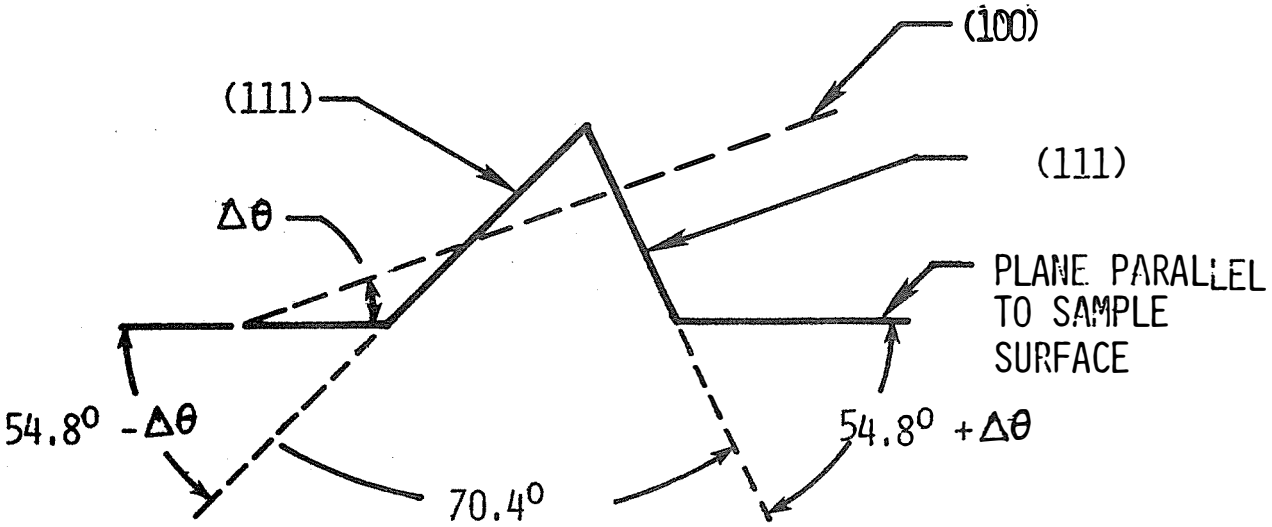

(B)

FIGURE 7: (A) ILLUSTRATION DEFINING ANGULAR OFF-SETS AND

(B) GRATING SHAPE (ALONG X-DIRECTION) DUE TO ANGULAR OFF-SET

recognition of twins. Characterization of twins by x-ray Laue analysis can be quite complex if each of the twinned grains is smaller than the x-ray beam, in which case the beam is incident on both at the same time. The inversion/reflection symmetry of the twinned grains with respect to the twin plane will be indicated by the symmetry of the diffraction patterns from either side of the twin plane. If the light is incident at the twin boundary and illuminates both grains, the diffraction pattern will exhibit the twin symmetry. Figure 8 shows a diffraction pattern due to a simple twin; it is clear that the surface plane is a (111) plane.

Diffraction patterns from an arbitrary orientation can, in general, appear complex. However, with a little experience it is possible to recognize reminiscent patterns of a low index orientation. Figure 9 shows diffraction patterns due to various grains in a polycrystalline ribbon sample grown by laser crystallization. This figure reveals a variety of patterns which can be traced to the basic (100) pattern. For example, patterns 2, 3, 11, and 12 are similar to that of Fig. 5, indicating an angular off-set with respect to (100). Other orientations are indicated on the figure.

We have determined orientations of the grains in Fig. 9 by the present optical as well as x-ray (Laue) techniques; results agree within 1 degree.

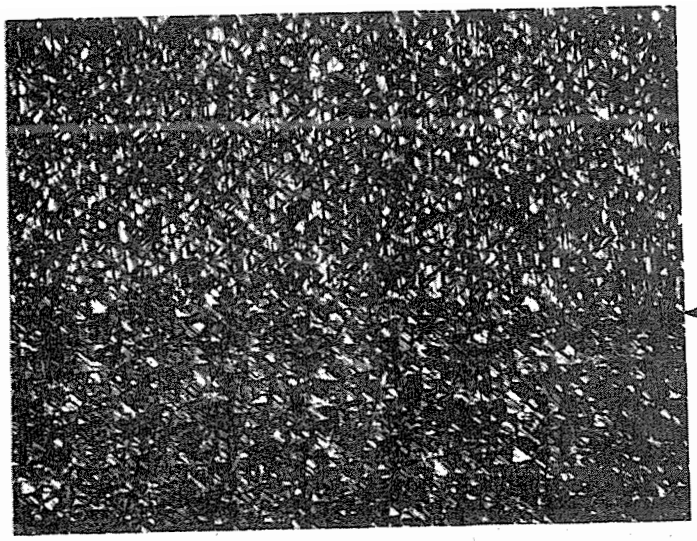

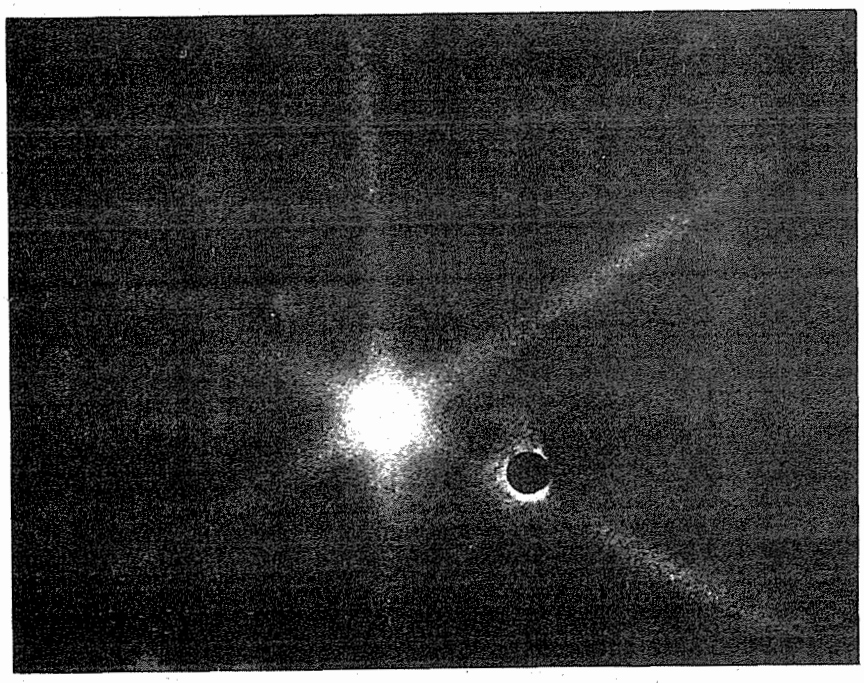

Figure 8: (a) Photograph of twinned grain and the boundary.

(b) Diffraction pattern resulting from illumination of twin boundary in (a).

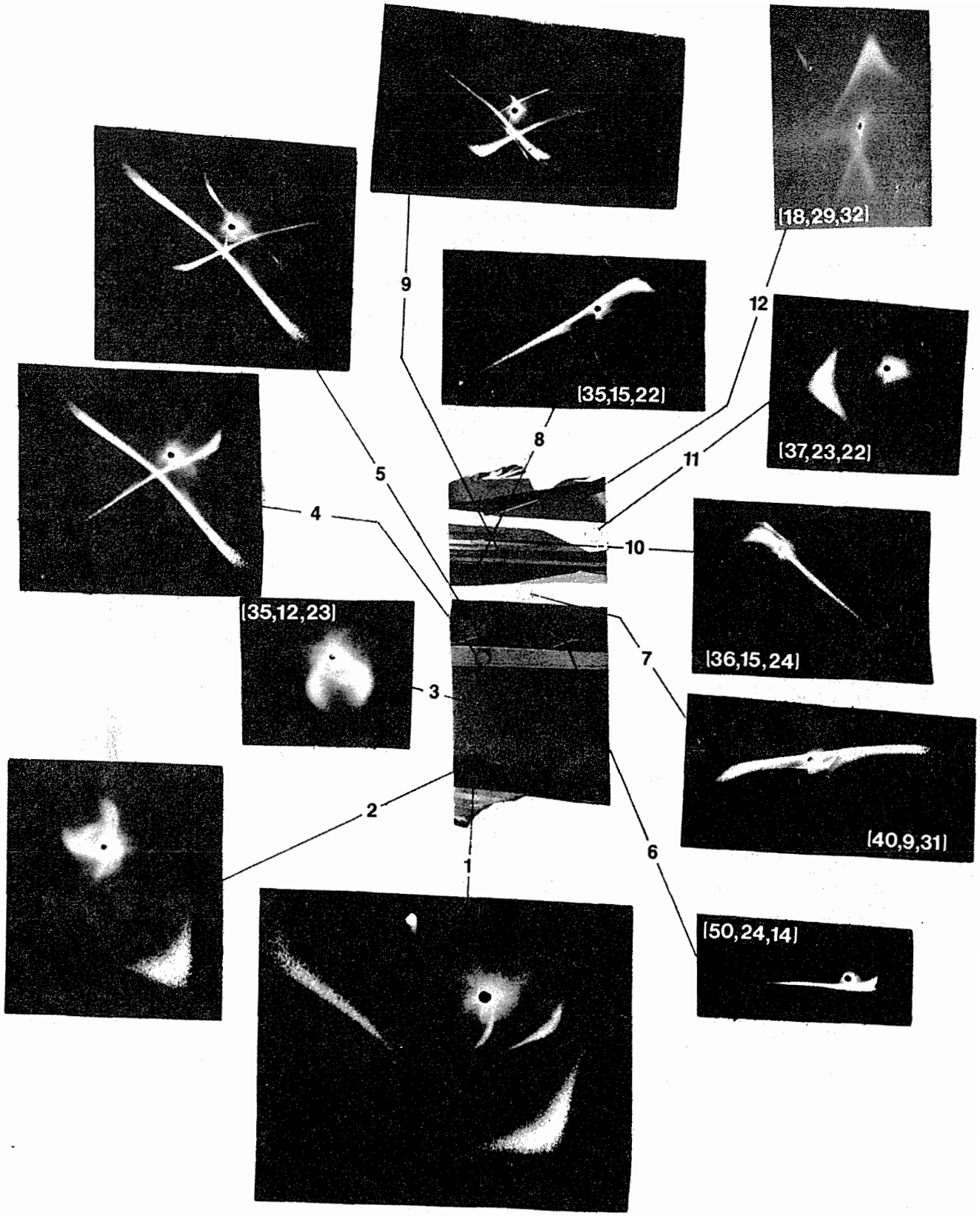

FIGURE 9: OPTICAL DIFFRACTION PATTERNS FROM VARIOUS GRAINS OF A LASER GROWN RIBBON. NUMBERS IN THE BRACKET INDICATE SURFACE ORIENTATION, IN DEGREES, WITH RESPECT TO (100), (110) and (111) PLANES, RESPECTIVELY.

5.0 GRAIN BOUNDARY ACTIVITY IN UNPROCESSED SUBSTRATES: THE TRANSVERSE PHOTOVOLTAGE (TPV) TECHNIQUE

A technique for determining G.B. "activity" in unprocessed substrates by utilizing optical excitation of carriers, has been studied. In this technique ohmic contacts are fabricated across the G.B. on the substrate surface, and a focussed laser beam (λ = 6328Å, or 1.15 μ) is scanned across the G.B. as shown in figure 10a. A typical signal, thus, generated at the contact is shown in figure 10b. The principle of operation and the application of this technique to the study of G.B. behavior are described in the following sections.

5.1 BASIC PRINCIPLE OF THE TECHNIQUE

The incident light beam creates electron-hole pairs within the semiconductor. In the absence of any lateral internal fields, these carriers recombine locally. However, when an internal field is present (such as due to a G.B. barrier or local changes in conductivity) electrons and holes are separated to generate a current (or voltage) signal at the terminals. The shape of the signal reflects the spatial variations in the internal field (related to the band bending). A theoretical analysis is now being carried out to determine spatial dependence of the internal field from the generated signal. Even without a detailed analysis, it is possible to relate (qualitatively) the signal to some grain boundary parameters.

1. Transverse fields on either side of the G.B. are in opposite directions (as seen from reversal in signal polarity) and
2. If we assume that the amplitude of the signal due to optical excitation is proportional to the local field, the field on either side of the G.B. is linear implying a parabolic band bending at the G.B.

It should be pointed out that carrier separation by the G.B. field will be influenced by recombination effects. The extent of this interaction depends

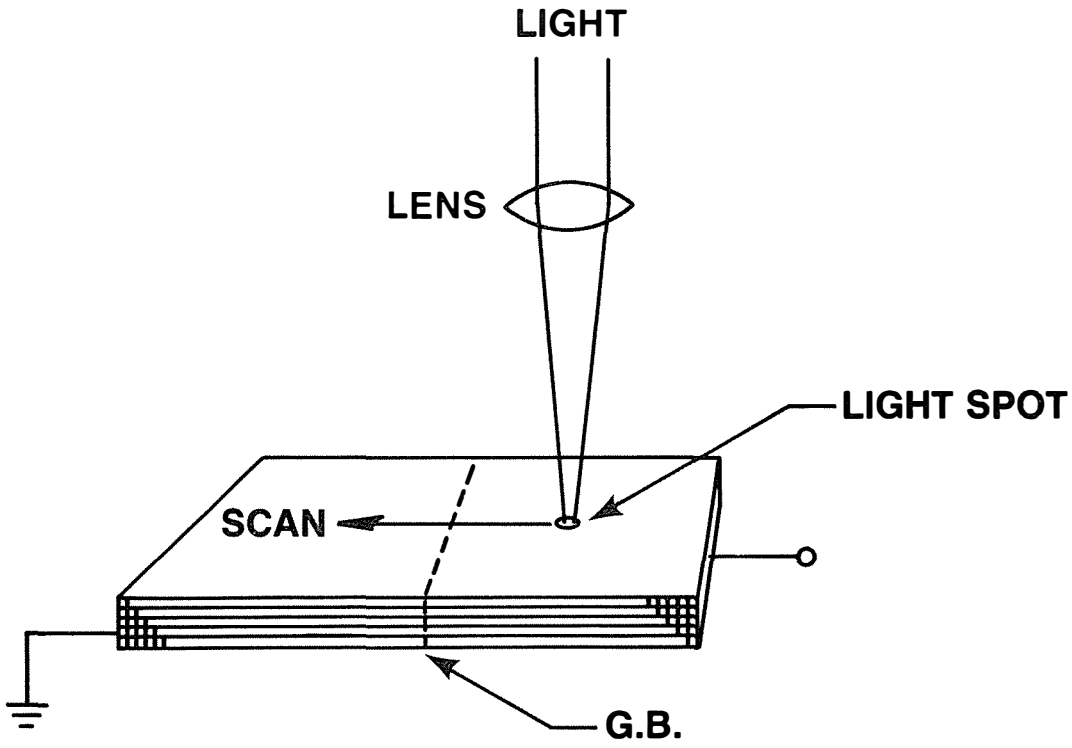

FIGURE 10A:

CONFIGURATION OF LIGHT SCAN ACROSS A G.B.

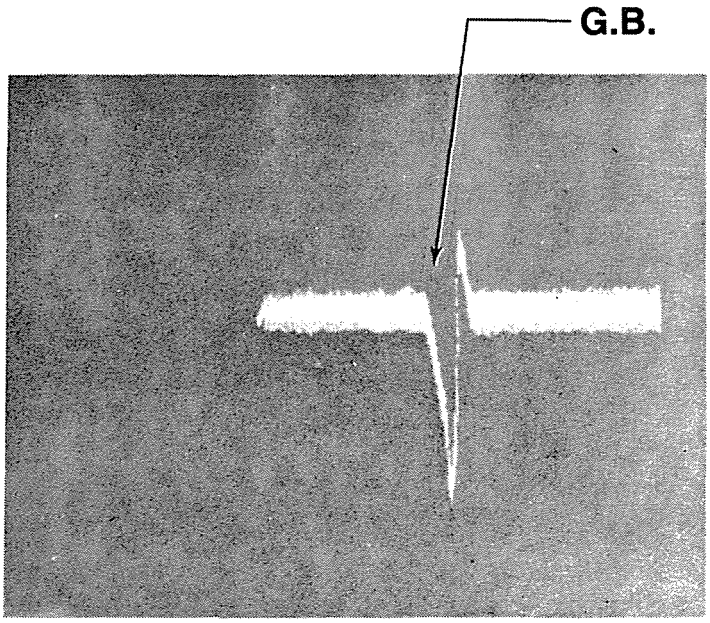

FIGURE 10B:

SIGNAL DUE TO LIGHT SCAN OF AN UNBIASED G.B.

F4352

on magnitude of the barrier and the intrinsic recombination velocity, S_o, associated with the G.B. Consequently the present technique appears to be well suited for evaluation of overall "activity" of a G.B., although other measurements may be necessary to separate effects of the G.B. barrier and S_o. It will be shown later in Section 5 that this technique is not sensitive to the presence of a high recombination region without any lateral field.

5.2 G.B. IMAGING

The above principle can be extended to image a G.B. in terms of its "activity" using a raster scanning, such as in a laser scanner. The following example demonstrates this G.B. imaging technique. A polycrystalline silicon sample (an RTR ribbon) was damage-free polished using the procedure described earlier (9). Ohmic contacts were fabricated on the polished side as shown in figure 11a. Because of polishing, G.B.s are not seen on the polished side; however, the transmission mode of an IR microscope can be used to photograph the G.B.s. Figure 11b is such a photograph showing G.B.s that run between two contacts. Figure 11c shows an image of the G.B. generated by scanning the region between contacts with a laser scanner. (An inversion in the G.B. images of figures 11b and 11c is due to the microscope.) An amplitude scan along the direction of the arrow in figure 11c, is given in figure 11d to indicate the relative signal levels at various positions along the G.B. Figure 11c shows an important result: G.B. "activity" may vary along the G.B. length. G.B. imaging can be very useful in evaluating influences of various processing steps on G.B. characteristics.

5.3 CORRELATION BETWEEN TPV AND VOLTAGE PICK-OFF

G.B. "activity" indicated by this (Transverse Photovoltage) technique is expected to have a good correlation with the transverse resistance indicated by a voltage

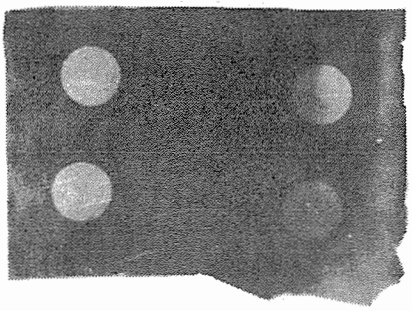

FIGURE 11a.
PHOTOGRAPH OF A POLISHED SAMPLE WITH METAL CONTACTS.

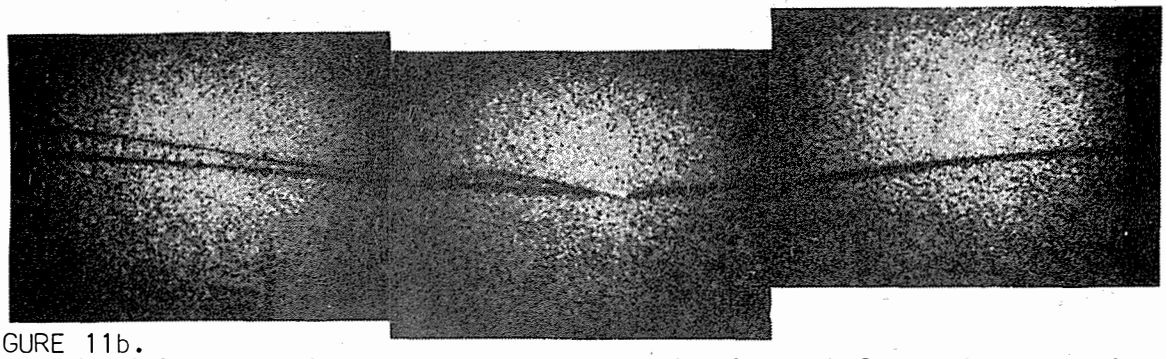

FIGURE 11b.
IR PHOTOGRAPH OF THE BACK (UNPOLISHED) SIDE OF THE SAMPLE SHOWING G.B.'s.

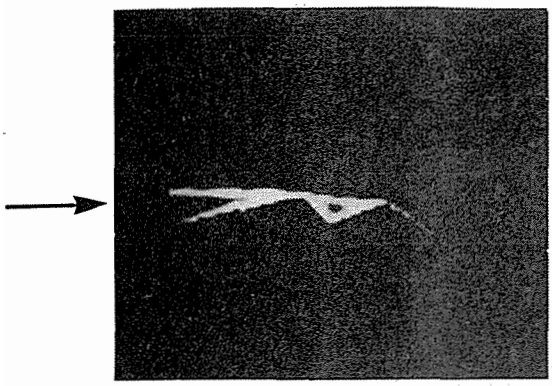

FIGURE 11c. **LIGHT SCAN IMAGE OF THE G.B.**

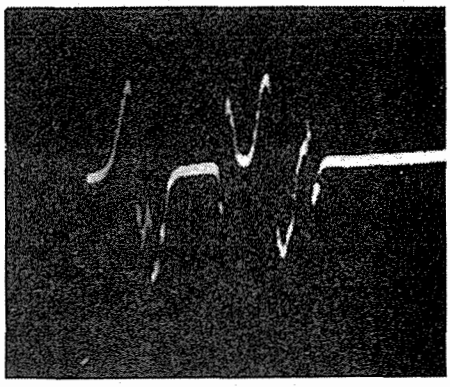

FIGURE 11d. **LINE SCAN SIGNAL ALONG THE ARROW IN ADJACENT PHOTOGRAPH.**

F4350

pick-off probe. To confirm this we have made both types of measurements in an RTR ribbon sample; figures 12a and 12b show these results. Voltage steps in figure 12a and the signal peaks in figure 12b occurring at the same G.B.s are identified by the same numbers. Figure 12c shows magnified signals of figure 12b. Two important results from figure 12 are: (i) G.B. activity is different at G.B.s 1, 2, and 3, and (ii) G.B. transverse resistance is well related to G.B. activity. Further analysis of this sample was carried out to determine source(s) that cause differences between the "activities" of various G.B.s. Results of these investigations are described in Section 6.

FIGURE 12a.

VOLTAGE PICK-OFF SCAN.

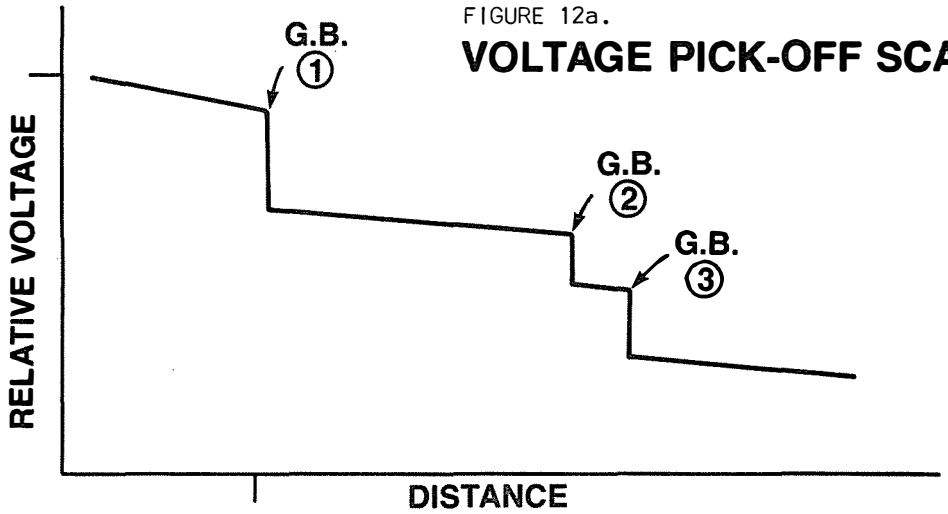

FIGURE 12b.

LIGHT SCAN SHOWING RELATIVE SIGNAL AT DIFFERENT G.B.s

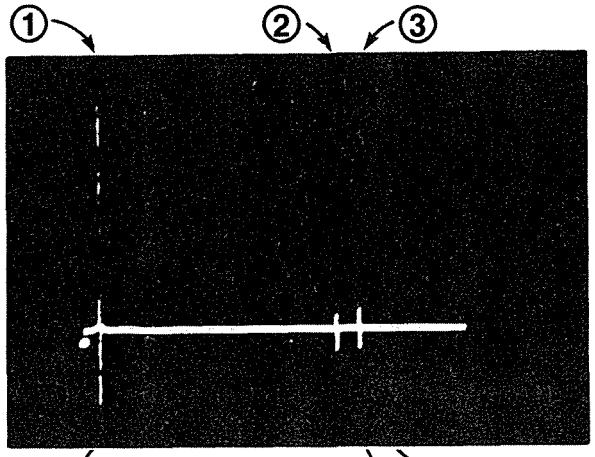

y-magnification = 1.2

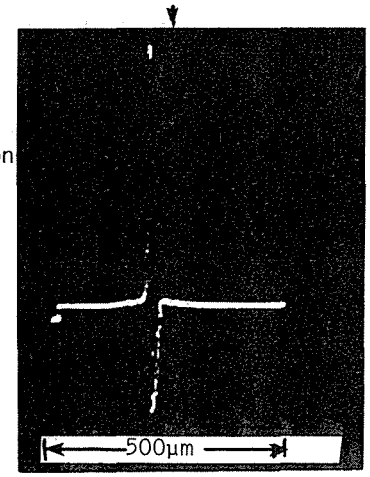

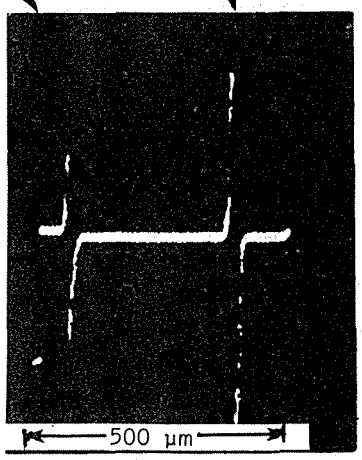

y-magnification = 5

FIGURE 12c. **HIGH RESOLUTION LINE SCANS NEAR G.B.'s.** F4351

6.0 GRAIN ORIENTATION AND G.B. MISFIT EFFECTS

We have initiated work towards evaluation of the dependence of G.B. characteristics on the relative orientation of the grains in RTR ribbons and large grain Wacker Silso. The aim of this study is to investigate the conditions under which G.B. properties do (or do not) correlate with the phenomeonolgical approach of a G.B. misfit. Results of this study are expected to be useful in three ways: (i) They will lead to a better understanding of G.B. effects in a large area device covering grains of different orientations (2) determine G.B. -- defect interaction mechanisms and (3) serve as a feedback for improvement of material quality (e.g. these results may indicate whether growth of certain orientations is more suitable for solar cells).

The basic approach of this study is as follows:

a. Determine G.B. activity and the region of G.B. influence as a function of G.B. misfit, in unprocessed substrates.

b. Fabricate small diodes within the grains and on G.B.s, and relate their performance to: (i) orientation and defect structure of grains (ii) G.B. misfit, respectively.

c. Correlate the results of (a) and (b) with physical characteristics of the G.B.s.

Our evaluation techniques are such that all the measurements can be done on the same samples, allowing unambiguous interpretation (which can otherwise occur) due to spatial variations in substrate characteristics.

Some preliminary experiments have been carried out with some very useful results. These are described as follows: Several samples were laser scribed from a ribbon (#1443A). Three adjacent samples which exhibited the same grain structure were selected for this study. Figure 13 shows schematically the grain propagation in these samples. Sample #4 was used for evaluation of G.B. activity (unprocessed) and measuring G.B. misfit; #3 and #5 were processed (as described in earlier reports) for diode fabrication.

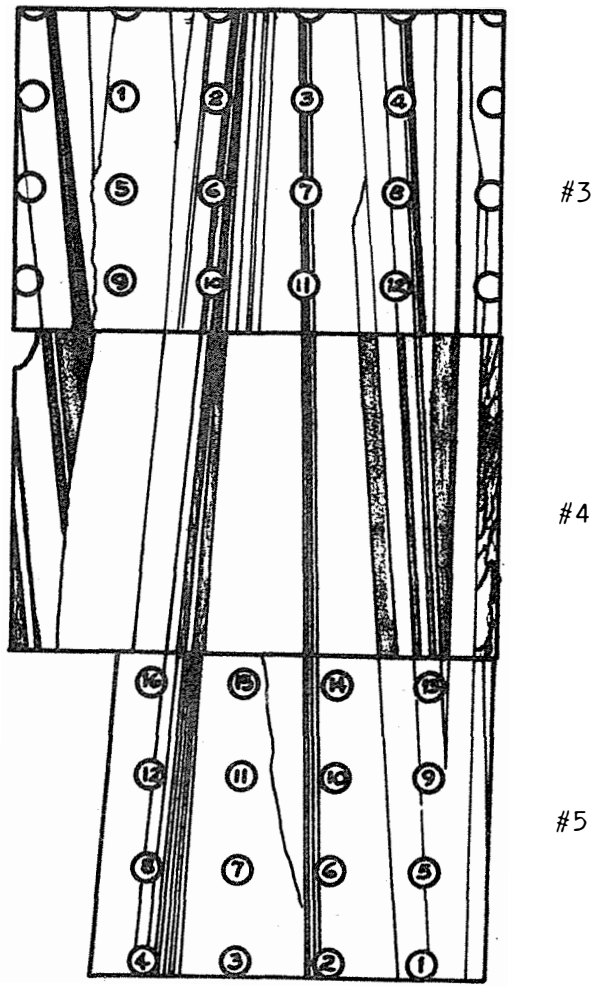

Figure 13: Schematic of grain propagation in three adjacent samples scribed from RTR ribbon #1443A.

FIGURE 14: Series of Nomarski photgraphs showing main structural features between contacts 3 and 4 of sample #1443A-4.

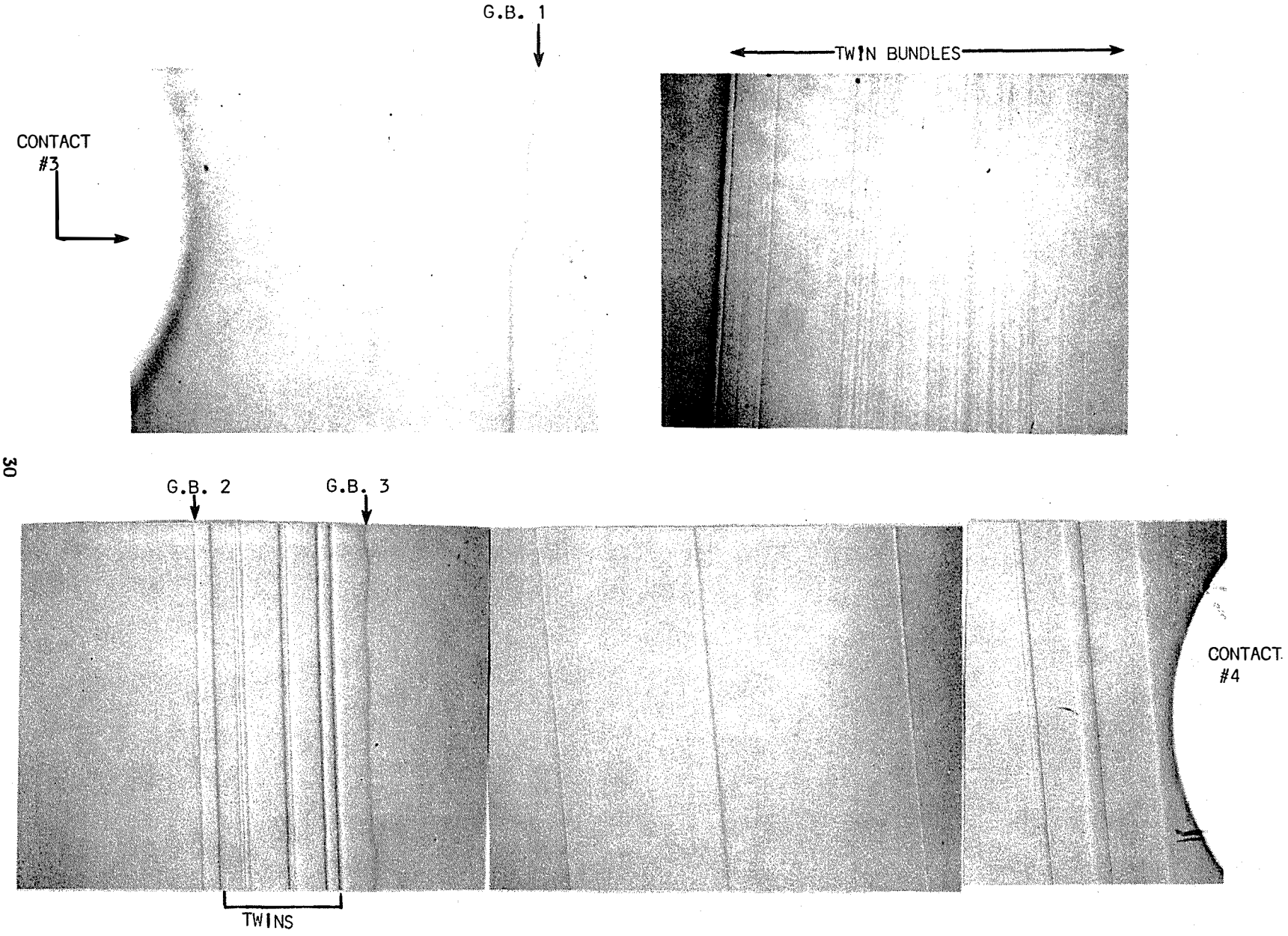

6.1 MISFIT EFFECTS ON G.B. ACTIVITY

Results of voltage pick-off and laser scanning on sample #4 were described in Section 5 (figure 12). We will now describe investigations carried out on the structure of the G.B.s to explain the differences in their activities. Figure 14 shows structure of the grains covered by the scans in figure 12 (i.e. between contacts) by a series of Nomarski photographs. This figure shows the presence of three major G.B.'s 1,2,3 and several twin bundles (the G.B.s corresponding to signals in figure 12 are similarly numbered). It is clear that the G.B.'s show significant electrical "activity" (as seen by these techniques) as compared to twin boundaries. These results may appear to contradict some results described in previous reports as to the photocurrent losses occurring at twin bundles. However, the explanation lies in the fact that in voltage pick-off and laser scanning (transverse photovoltaic) techniques the dominant contribution to the signal is due to the barrier height and that regions of high recombination (without any appreciable transverse fields) are inactive. Hence it may be concluded that the twin boundaries (in figure 14) do not show any barrier height effects. Further discussion on recombination occurring at twin boundaries is given in Section 6.2.

Electrical activity, A, of the G.B.'s varies as $A_{G.B.1} > A_{G.B.3} > A_{G.B.2}$. To determine if A is related to G.B. misfit, the sample was texture etched in order to determine the grain orientations by the optical diffraction technique. Figure 15a is a photograph of the textured sample showing individual grains.

In order to simplify the description of the G.B. misfit let us consider some general featues of grain orientations in RTR ribbons. We have observed that surface orientations are close to a (110) plane. Hence, grain orientations may be described as angular deviations, θ and ϕ, of the grain surface from the (110) plane along orthogonal directions as shown in figure 15b. A third component of misorientation is tilt δ of the [110] direction in the surface plane. Table 1 shows measured values of various misfit angles for the G.B.s in figure 15a.

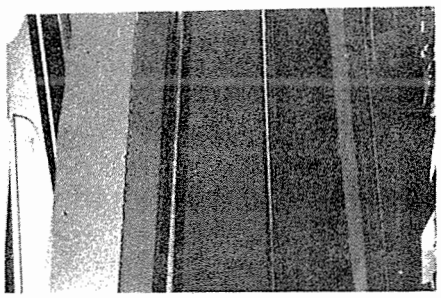

(a)

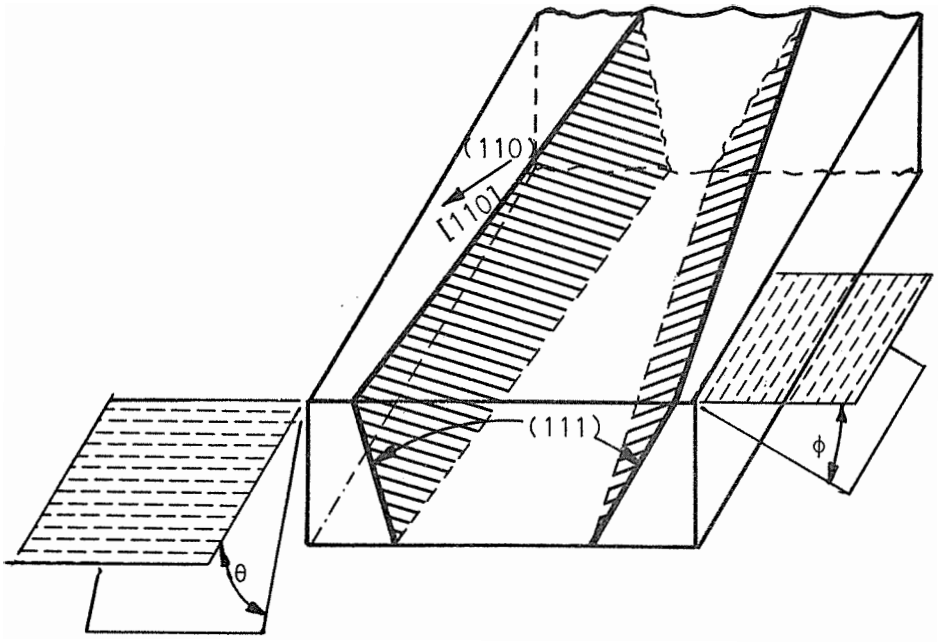

(b)

FIGURE 15: a) Photograph of sample #3 after texture etching shows various grains and G.B.s.
b) A schematic showing general orientations in RTR ribbons.

TABLE 1

G.B. MISFITS AS MEASURED BY THE OPTICAL TECHNIQUE

G.B. #	θ°	ϕ°	δ°
1	0	9	1
2	0	1	0
3	0	3	0

It may thus be concluded that G.B. activity is well related to G.B. misfit. However, it should also be emphasized that (as seen from Table 1) their dominant misfit component is due to tilt.

6.2 INFLUENCE OF G.B. MISFIT ON CELL CHARACTERISTICS

In order to further analyze the effects of grain orientations and G.B. misfit, diodes were fabricated on samples #3 and #5. Figures 16a and 16b show photographs of these samples after fabricating diode arrays -- the substrate structure underneath the diodes is revealed by mesa etching. As described previously (9), a slight delineation of defects and G.B.s is an important characteristic of the etchant developed for this purpose, which helps in selection of appropriate diodes for various measurements. The diodes in figure 16 are 100 mils in diameter with a center-to-center separation of 300 mils*. Although no diodes are located on G.B. 1, some important results can still be inferred from the diodes located on dislocation boundaries (D.B.'s) and twin boundaries.

Table 2 shows cell parameters of various diodes on sample #3. From these data and the substrate structure, we can arrive at the following conclusions.

1. Diodes 1, 5, and 9 (sample #3) all located on dislocation boundary D.B. 2, exhibit low V_{OC}s and J_{SC} (in particular J_{SC}). Furthermore, the influence of the proximity of D.B.1 is seen as a progressive lowering in cell parameters, i.e. in the order D_9, D_5, D_1.
2. D_4, D_8, and D_{12} show degradation due to the influence of non-parallel twins. (Low value of V_{OC} in D_8 is due to a surface scratch.)

---

*This diode pattern was mistakenly fabricated. The array pattern intended for this study consists of 50 mil diameter diodes with a center-to-center separation of 100 mils; such a pattern would have resulted in some diodes on G.B.s 1, 2, and 3. Accordingly the study on these diodes was directed at the effects of other types of defects.

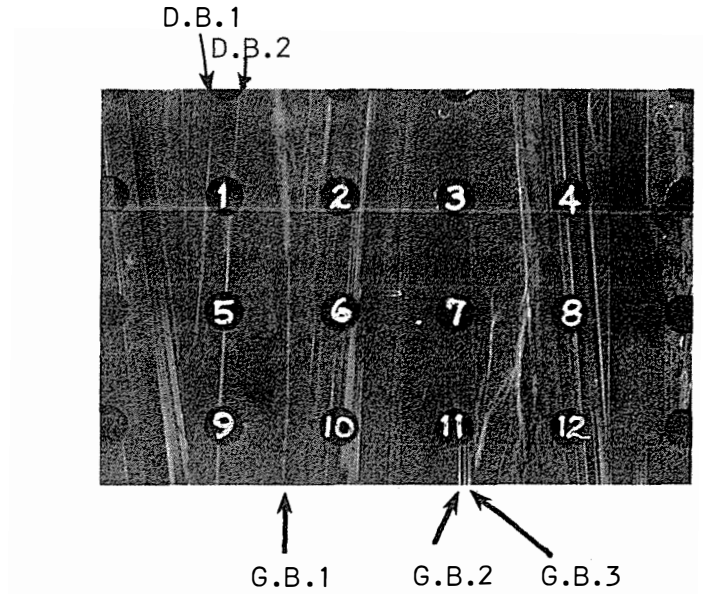

SAMPLE #3
(a)

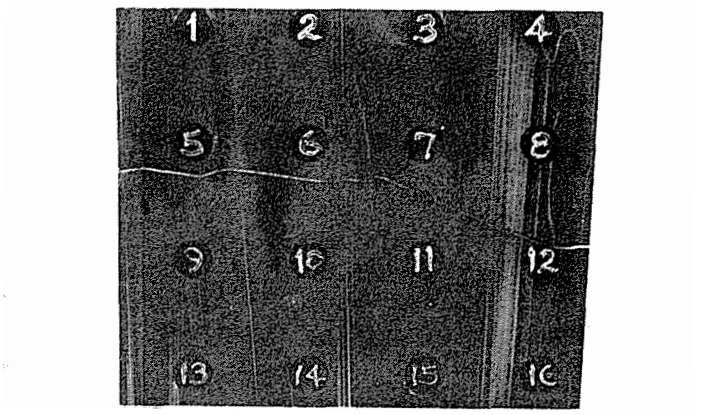

SAMPLE #5
(b)

Figure 16: Photographs of samples 3 and 5 after diode fabrication showing underlying substrate structure.

TABLE 2

CELL PARAMETERS, V_{OC} AND J_{SC}, OF DIODES ON SAMPLE #3.

SAMPLE #3

DIODE #	V_{OC} mV	J_{SC} mA/cm^2
1	552	16.92
2	558	17.63
3	561	20.91
4	535	18.13
5	561	17.42
6	555	18.43
7	586	22.17
8	236	17.93
9	572	18.18
10	561	19.44
11	571	21.21
12	560	16.72

3. D_3, D_7 and D_{11} are located on G.B.2. Other features of these diodes are: (a) G.B.3 runs under D_3 and in close proximity of D_{11}. (b) Grain to the left of G.B.2 has low dislocation density, and (c) region between G.B.2 and G.B.3 predominantly consists of parallel twins. Performance of these diodes clearly shows that G.B. 3 has stronger degradation effects than G.B.2.

4. A comparison of log I vs V plots of D_7 and D_{12}, shown in figure 17, indicate that loss in cell parameters is due to an increase in dark current associated with non-parallel twins.

Similar conclusions can be arrived at from laser scan analysis of the diodes. For example figure 18a shows a line scan of the photocurrent response on D_{10}. Figure 18b shows the substrate structure underlying D_{10} (inverted placement of the photographs is for convenience in identifying various regions corresponding to the photoresponse). Corresponding regions in figure 18a and 18b are labelled. The following observations can be made from these figures.

(i) Dislocation boundaries result in photocurrent loss.

(ii) Parallel twins constitute regions of high photocurrent.

(iii) Non-parallel twins show photocurrent loss.

Cell parameters of diodes on sample #5 are given in Table 3. A correlation of cell parameters with diode structure leads to results similar to those obtained from sample #3.

FIGURE 17: DARK LOG I vs. V PLOTS OF D_7 AND D_{12}

● - D_{12}

o - D_7

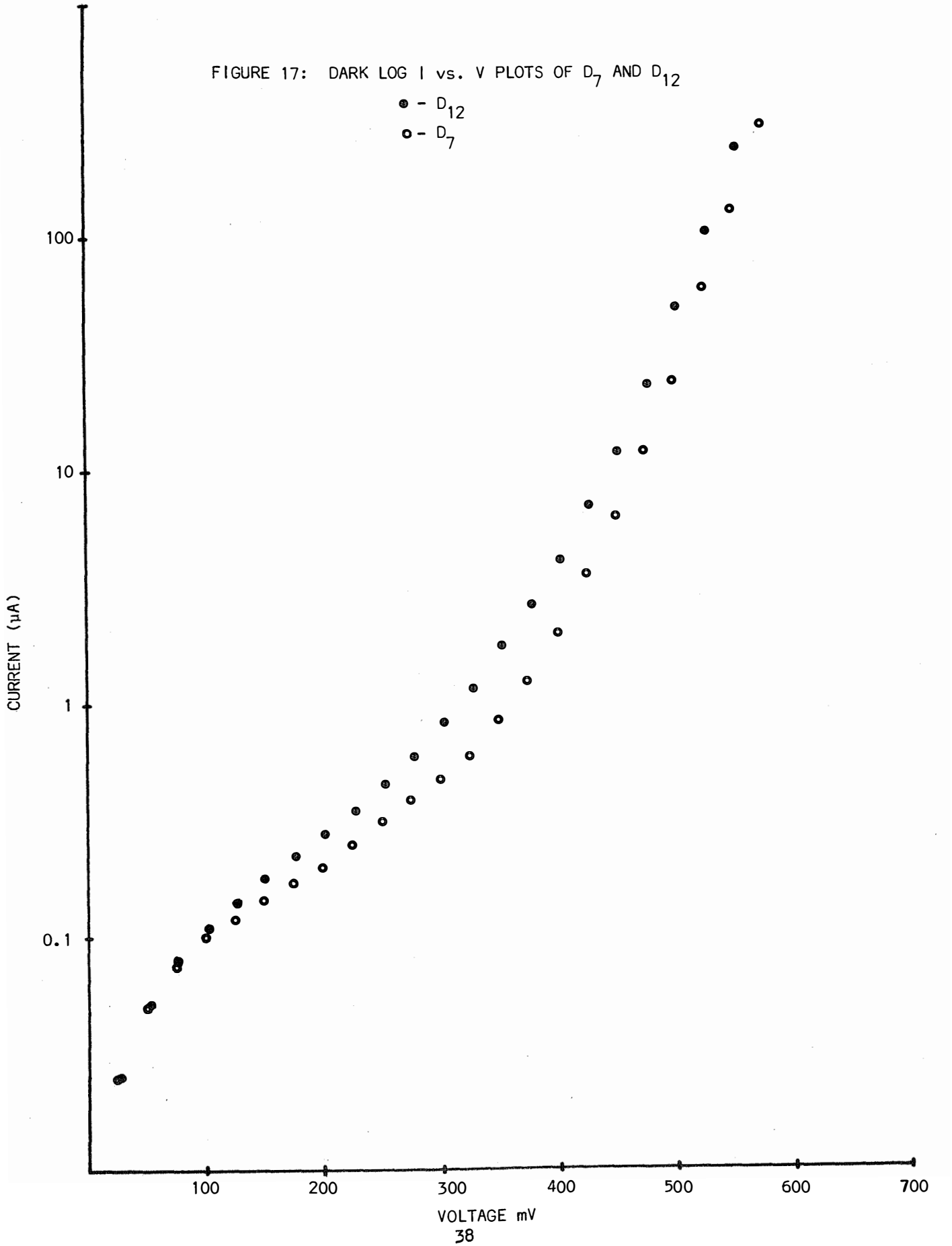

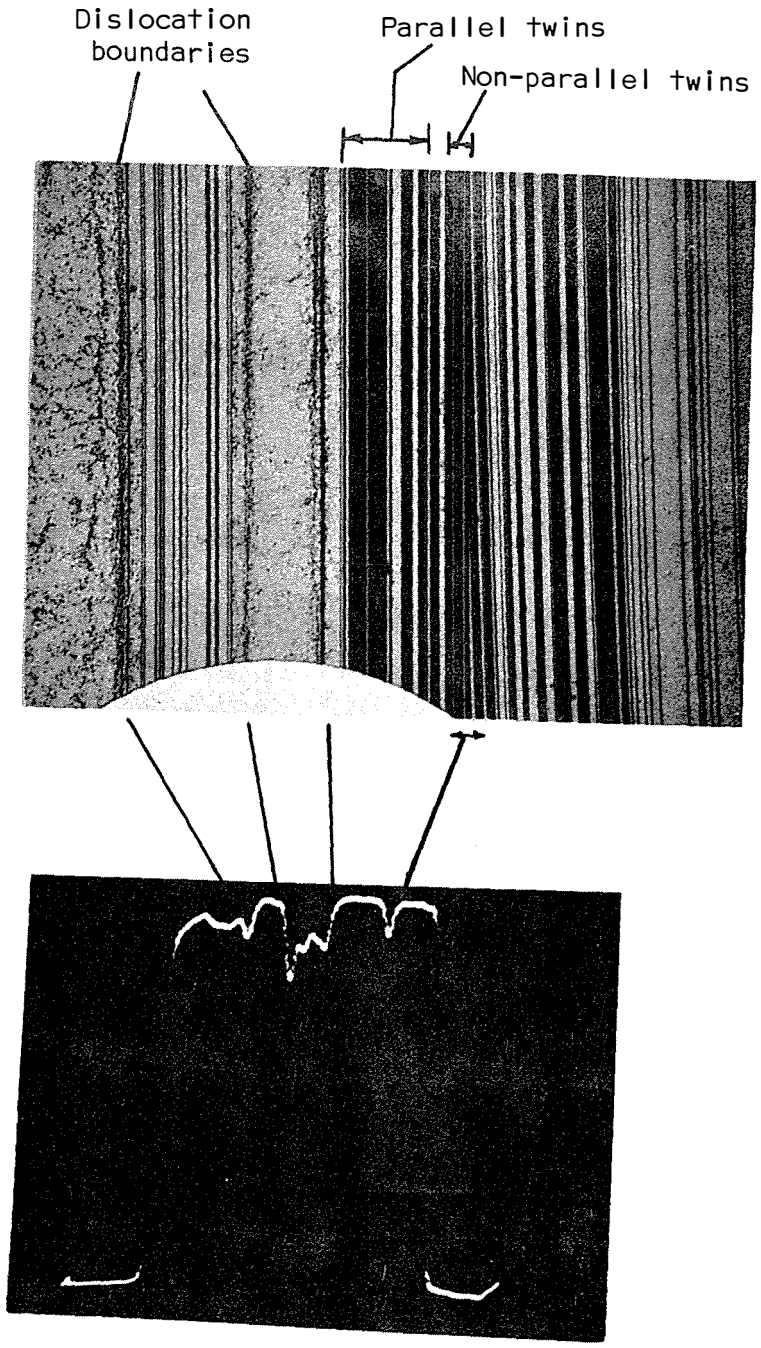

FIGURE 18. a) Line scan showing photocurrent losses at various G.B.s on D_{10}
b) Structure of D_{10}.

TABLE 3

CELL CHARACTERISTICS OF DIODES ON SAMPLE #1443A-5

DIODE #	V_{OC}	J_{SC}
1	575	19.14
2	566	16.92
3	572	17.27
4	435	22.73
5	575	18.28
6	567	16.97
7	569	17.27
8	576	19.65
9	399	18.69
10	505	17.22
11	560	17.58
12	---	---
13	550	19.7
14	548	18.18
15	565	17.93
16	550	16.97

7.0 CONCLUSIONS

We have studied several techniques for analyzing influences of defects/G.B. on photovoltaic performance. Advantages offered by these techniques are:

1. Ease in determining grain orientations.
2. Influences of grain orientations on cell performance (via defect generation) can be determined.
3. Effects of G.B. barrier and intrinsic recombination can be isolated.
4. All measurements can be done on the same sample (even the same region) of a sample, thereby minimizing any ambiguities which might arise if measurements are done in different regions of the sample (due to spatial non-uniformities).

Initial results have shown:

1. A good correlation exists between G.B. misfit and G.B. "activity".
2. Twin boundaries do not show existance of any appreciable barrier.
3. Very low angle (dislocation) boundaries are strong recombination carriers with no measureable barrier.
4. Parallel twins are, in general, regions of low dislocation density resulting in high photoresponse.
5. Non-parallel twins show low photoresponse. Although exact mechanism(s) responsible for this loss are not established yet, we have shown earlier (9) that non-parallel twins are regions of high residual stress.
6. G.B. "activity" may vary along its length.

We have also shown that small diode analysis can be used to isolate the effects of a G.B. and twin boundaries on cell parameters.

In the future, these techniques will be applied to more polycrystalline silicon samples to study a wider range of G.B. misfits and their associated "activity" and photovoltaic losses.

REFERENCES

1. G. H. Schwuttke, J. Elec. Chem. Soc., 106, 315 (1959).
2. R. C. Ellis, Jr., J. Appl. Phys., 25, 1497 (1954).
3. W. L. Bailey et. al. U.S. Patent 4,137,123. Jan. 1979.
4. M. J. Declencg et al. J. Elec. Chem. Soc., 122, 545, (1975).
5. C. R. Baraona et al., Proceedings 11th IEEE Photovoltaic Specialists Conference, 44 (1975).
6. B. L. Sopori, "Optical Characteristics of Textured Silicon Surfaces" to be published.
7. Notice that the diffraction pattern gives the orientation of the surface as well as one direction in the surface plane.
8. For example see F. A. Jenkins and H. E. White, Fundamentals of Optics, Third Edition, McGraw-Hill, N.Y. 1957.
9. B. L. Sopori, "Photovoltaic Mechanisms in Polycrystalline Thin Film Silicon Solar Cells", Final Report, DOE Contract #AC-01-79ET-23104.

☆ U.S. GOVERNMENT PRINTING OFFICE: 1981-740-145/1256